Cellular/Molecular

$Ca_V1.3$ Channels Are Essential for Development and Presynaptic Activity of Cochlear Inner Hair Cells

Andreas Brandt,[1] Joerg Striessnig,[2] and Tobias Moser[1]

[1]Department of Otolaryngology, Goettingen University Medical School, 37075 Goettingen, Germany, and [2]Department of Pharmacology and Toxicology, Institute of Pharmacy, University of Innsbruck, A-6020 Innsbruck, Austria

Cochlear inner hair cells (IHCs) release neurotransmitter onto afferent auditory nerve fibers in response to sound stimulation. During early development, afferent synaptic transmission is triggered by spontaneous Ca^{2+} spikes of IHCs, which are under efferent cholinergic control. Around the onset of hearing, large-conductance Ca^{2+}-activated K^+ channels are acquired, and Ca^{2+} spikes as well as the cholinergic innervation are lost.

Here, we performed patch-clamp measurements in IHCs of mice lacking the $Ca_V1.3$ channel ($Ca_V1.3^{-/-}$) to investigate the role of this prevailing voltage-gated Ca^{2+} channel in IHC development and synaptic function. The small Ca^{2+} current remaining in IHCs from 3-week-old $Ca_V1.3^{-/-}$ mice was mainly mediated by L-type Ca^{2+} channels, because it was sensitive to dihydropyridines but resistant to inhibitors of non-L-type Ca^{2+} channels such as ω-conotoxins GVIA and MVIIC and SNX-482. Depolarization induced only marginal exocytosis in $Ca_V1.3^{-/-}$ IHC, which was solely mediated by L-type Ca^{2+} channels, whereas robust exocytic responses were elicited by photolysis of caged Ca^{2+}. Secretion triggered by short depolarizations was reduced proportionally to the Ca^{2+} current, suggesting that the coupling of the remaining channels to exocytosis was unchanged.

$Ca_V1.3^{-/-}$ IHCs lacked the Ca^{2+} action potentials and displayed a complex developmental failure. Most strikingly, we observed a continued presence of efferent cholinergic synaptic transmission and a lack of functional large-conductance Ca^{2+}-activated K^+ channels up to 4 weeks after birth. We conclude that $Ca_V1.3$ channels are essential for normal hair cell development and synaptic transmission.

Key words: **calcium channel; hair cell; afferent; efferent; BK channel; development**

Introduction

Inner hair cells (IHCs) of the cochlea are mechanosensory cells that transform mechanical stimuli into neuronal signals. In contrast to other presynaptic elements, hair cell neurotransmission is thought to mainly rely on L-type Ca^{2+} channels (Fuchs et al., 1990; Roberts et al., 1990; Moser and Beutner, 2000; Platzer et al., 2000; Spassova et al., 2001). In addition, L-type Ca^{2+} channels may have a role in hair cell development. Before the onset of hearing, IHCs fire Ca^{2+} action potentials (APs) (Kros et al., 1998; Glowatzki and Fuchs, 2000; Beutner and Moser, 2001), which drive afferent synaptic transmission (Beutner and Moser, 2001; Glowatzki and Fuchs, 2002). This presensory activity is probably important for the development and maintenance of the auditory pathway (Tierney et al., 1997; Mostafapour et al., 2000).

The activity of IHCs is modulated by efferent cholinergic synaptic input (Glowatzki and Fuchs, 2000) from the superior olive (Pujol, 1985; Simmons et al., 1996; Bruce et al., 2000), probably shaping the IHC output to cause a bursting activity pattern in the auditory nerve (Lippe, 1994; Walsh et al., 1998). Acetylcholine (ACh) release causes Ca^{2+} influx through nicotinic alpha9/10 receptors (Elgoyhen et al., 1994, 2001), which in turn activates a hyperpolarizing current through small-conductance Ca^{2+}-activated K^+ channels in hair cells (Housley and Ashmore, 1991; Fuchs and Murrow, 1992; Glowatzki and Fuchs, 2000; Oliver et al., 2000). However, most efferent fibers retract from the IHCs and synapse onto afferent dendritic endings beneath the IHCs during normal development (Pujol, 1985; Simmons et al., 1996).

Bursts of APs result in oscillatory changes in cytosolic free Ca^{2+} ($[Ca^{2+}]_i$) of IHCs (Beutner and Moser, 2001), which, by analogy to other cells (Spitzer et al., 1995; Dolmetsch et al., 1998), could be important signals for gene expression. IHCs undergo major changes in their expression of potassium channels (Kros et al., 1998; Marcotti et al., 2003), calcium channels (Beutner and Moser, 2001), and synaptic proteins (Eybalin et al., 2002) during development. Some of these important events, like the acquisition of large-conductance Ca^{2+}-activated K^+ channels (BK channels) around the onset of hearing, rely on functional thyroid hormone signaling (Rusch et al., 1998).

Here, we performed whole-cell recordings of membrane current, potential, and capacitance of $Ca_V1.3^{-/-}$ mice (Platzer et al., 2000) to study the effect of a strongly reduced Ca^{2+} channel density on development and function in IHCs. $Ca_V1.3^{-/-}$ mice are deaf and finally undergo degeneration of afferent auditory

Received July 16, 2003; revised Sept. 29, 2003; accepted Sept. 29, 2003.

This work was supported by Deutsche Forschungsgemeinschaft grants (SFB 406: synaptic part; CMPB: developmental part) to T.M. and Austrian Science Fund Grant P-14820 and European Community Grant HPRN-CT-2000-00082 to J.S. We thank D. Oliver, T. Sakaba, R. Schneggenburger, R. Nouvian, and S. Patel for their comments on this manuscript and M. Köppler for excellent technical assistance. We also thank W. Steiner and E. Neher for their continued support.

Correspondence should be addressed to Tobias Moser, Department of Otolaryngology, Goettingen University Medical School, Robert-Koch-Strasse 40, 37075 Goettingen, Germany. E-mail: tmoser@gwdg.de.

 0270-6474/03/2310832-09$15.00/0

Table 1. Passive electrical properties of $Ca_V1.3^{-/-}$ and wt IHCs at the different postnatal ages

	V_m (mV)	C_m (pF)	R_s (MΩ)	R_{in} (GΩ)
wt, P5–P10	−70.1 ± 1.1 ($n = 4$)	7.6 ± 0.2 ($n = 18$)	13.2 ± 1.4 ($n = 16$)	1.87 ± 0.2 ($n = 12$)
$Ca_V1.3^{-/-}$, P6–P10	−56.1 ± 2.4 ($n = 11$)	6.9 ± 0.2 ($n = 30$)	13.0 ± 1.0 ($n = 30$)	1.66 ± 0.2 ($n = 15$)
$Ca_V1.3^{-/-}$, P17–P39	−71.0 ± 1.8 ($n = 16$)	6.7 ± 0.09 ($n = 90$)	wc: 11.5 ± 0.5 ($n = 68$) pp: 19.1 ± 1.7 ($n = 22$)	2.6 ± 0.2 ($n = 73$)
wt, P24–P31	−77.1 ± 0.7 ($n = 15$)	12.0 ± 0.57 ($n = 17$)	12.7 ± 1.6 ($n = 17$)	0.40 ± 0.05 ($n = 9$)

The data represent mean ± SEM for resting membrane potential (V_m), membrane capacitance (C_m), series resistance [R_s, uncompensated, estimated at 3 min after establishing the whole-cell configuration (wc) or reaching <30 MΩ for perforated-patch (pp)], and input resistance (R_{in}) at the different developmental ages pooling over all experiments, except for V_m which was measured in current clamp using solutions II_i and III_e.

nerve fibers and hair cells (Platzer et al., 2000). Their early postnatal IHCs display a 90% reduction of the Ca^{2+} current. We show that the absence of $Ca_V1.3$ channels abolishes postnatal Ca^{2+} spiking and impairs IHC development. Thus, $Ca_V1.3^{-/-}$ IHCs lacked BK channels and kept their efferent cholinergic innervation up to at least the fourth postnatal week. Depolarization-induced exocytic increases of membrane capacitance (C_m) were strongly reduced. This afferent synaptic dysfunction would itself be sufficient to cause the deafness of the mutants and probably is at the origin of afferent fiber degeneration.

Materials and Methods

Patch-clamp recordings. $Ca_V1.3^{-/-}$ mice (Platzer et al., 2000) (mice were backcrossed for at least five generations into a C57BL/6N genetic background) or wild-type mice (wt) (C57BL/6J) of the specified age (see figure legends) were killed by decapitation, according to national ethical guidelines. IHCs from the apical coils of freshly dissected organs of Corti were patch-clamped at their basolateral face at room temperature (20–25°C).

Pipette solutions contained (in mM): solution I_i: 150 Cs-gluconate, 13 TEA-Cl, 10 CsOH-HEPES, 1 $MgCl_2$, 2 MgATP, and 0.3 NaGTP, pH 7.2, for Ba^{2+}–Ca^{2+} current and capacitance measurements; solution II_i: 150 KCl, 2 $MgCl_2$, 10 KOH–HEPES, and 2.5 MgATP, pH 7.3, for recordings of K^+ currents, APs, mechanoelectrical transduction (MET), and postsynaptic currents/potentials; for some AP and postsynaptic current measurements, KCl was replaced by equimolar K^+-gluconate; solution III_i: 120 Cs-gluconate, 20 TEA-Cl, 20 CsOH-HEPES, 10 DM-nitrophen, 10 $CaCl_2$, 5 1,3-diamino-2-propanol-*N*,*N*,*N*′,*N*′-tetraacetic acid, and 1 Furaptra, pH 7.2, for flash photolysis.

Perforated-patch recordings were performed using amphotericin B (Calbiochem, La Jolla, CA) (final concentration up to 250 μg/ml). For standard whole-cell experiments 50 μM Ca^{2+}-free and 50 μM Ca^{2+}-loaded EGTA were added to the pipette unless stated otherwise in the legends. All pipette solutions had osmolarities between 300 and 320 mmol/l.

The extracellular solutions contained (in mM): solution I_e: 105 NaCl, 35 TEA-Cl, 2.8 KCl, 10 $CaCl_2$, 1 $MgCl_2$, 10 NaOH-HEPES, and 10 D-glucose for Ca^{2+} current and capacitance measurements; solution II_e: 95 NaCl, 35 TEA-Cl, 2.8 KCl, 20 $BaCl_2$, 1 $MgCl_2$, 10 NaOH-HEPES, and 10 D-glucose for Ba^{2+}-current recordings; solution III_e: 137 NaCl, 5.8 KCl, 10 $CaCl_2$, 0.9 $MgCl_2$, 10 NaOH-HEPES, and 10 D-glucose for all other experiments.

Extracellular solutions were adjusted to pH 7.2 for solutions I_e and II_e and to pH 7.3 for solution III_e and had osmolarities between 300 and 320 mmol/l. Dihydropyridines (DHPs) (Isradipine, kindly provided by Novartis, Basel, Switzerland; BayK8644, Sigma St. Louis, MO) were dissolved in DMSO (Fluka, Buchs SG, Switzerland) or ethanol at 10 mM concentration and stored below −25°C. Stock solutions of toxins (ω-conotoxins MVIIC and GVIA; Bachem Biochemica GmbH, Heidelberg, Germany; SNX-482, Peptide Institute Inc., Osaka, Japan) and Dequalinium (Tocris Cookson, Ellisville, MO) were stored below −25°C in double-distilled water. Tetraethylammonium (TEA)-chloride was obtained from Fluka; fura-2, Furaptra, DM-Nitrophen, and FM1–43 were from Molecular Probes (Eugene, OR). All other chemicals were obtained from Sigma. Before the experiments, the drugs were diluted to their final concentration (see figure legends, solvents not exceeding 0.1%). Solution changes were achieved by bath exchange or by a local large-tip perfusion pipette. Cells were voltage- or current-clamped and stimulated electrically or by flash photolysis except for MET recordings, in which a piezo-driven fluid-jet-stimulation was used (similar to Meyer et al., 1998). Flash photolysis was performed as described in Beutner et al. (2001). In brief, we combined short (~1 msec) flashes of ultraviolet light from a Xenon arc flash lamp (Rapp OptoElectronics, Hamburg, Germany) and subsequent UV-illumination by a polychromatic light source (TILL Photonics, Martinsried, Germany) to obtain step-wise increases in $[Ca^{2+}]_i$.

Data acquisition and analysis. EPC-9 amplifiers (HEKA, Lambrecht, Germany) controlled by "Pulse"-software (HEKA) were used for measurements and acquisition. Currents were sampled at 20–40 kHz and low-pass filtered at 2–5 kHz. We measured C_m using the Lindau–Neher technique (Lindau and Neher, 1988), implemented in the software-lockin module of "Pulse." A 1 kHz, 70 mV peak-to-peak sinusoid was applied around a DC holding potential of −80 mV. For the impedance analysis the reversal potential of the DC current was set to the reversal potential of the slow tail currents following the depolarizations as described before (Moser and Beutner, 2000). For K^+ current measurements, R_s compensation was used (50–60%), and data were off-line corrected for the remaining voltage error. All K^+ currents were leak-corrected using a P/6-protocol. Leak subtraction for Ca^{2+}/Ba^{2+} currents was performed off-line, by subtracting a linear function approximating the current–voltage (*I–V*) relationship up to ~10 mV below the Ca^{2+} channel activation range for each individual *I–V*. Table 1 summarizes the average passive electrical properties of $Ca_V1.3^{-/-}$ and wt IHCs at the different postnatal ages.

All experimental data were analyzed using IgorPro software (Wavemetrics, Lake Oswego, OR). Membrane capacitance increment (ΔC_m) was estimated as the difference of the mean C_m after the end of the depolarization and the mean prepulse C_m (the initial 40 msec after the depolarization were skipped). All voltages were corrected for liquid junction potentials. K^+ currents were analyzed by averaging time windows at 1.2 msec for 100 μsec (early) and at 140 msec for 9.5 msec (late) of the time of depolarization for Figure 4*D* and by mono-exponential or double-exponential fitting (data not shown). Means are expressed ± SEM and were compared for statistical differences using the unpaired *t* test.

Results

Impaired stimulus–secretion coupling in $Ca_V1.3^{-/-}$ mice

Figure 1*A* displays Ca^{2+} currents of representative 3-week-old wt and $Ca_V1.3^{-/-}$ IHCs elicited by depolarization to the peak Ca^{2+} current potential. The average current–voltage functions of the Ca^{2+} currents recorded from wt IHCs ($n = 6$ cells; hearing: p20–32) and $Ca_V1.3^{-/-}$ IHCs ($n = 7$ cells; p14–32) are compared in Figure 1*B*. Together, the data demonstrate the dramatic reduction of the Ca^{2+} current after genetic ablation of $Ca_V1.3$ (~92%). Exocytosis, recorded as membrane capacitance increments (ΔC_m) in response to depolarizations of different durations, was similarly reduced in $Ca_V1.3^{-/-}$ cells (Fig. 1*C*,*D*). Two kinetic components of exocytosis can be discriminated in IHCs, with the fast one (up to ~20–30 msec of stimulation) mainly representing exocytosis of the readily releasable pool of synaptic vesicles (RRP) (Moser and Beutner, 2000). $Ca_V1.3^{-/-}$ IHCs still displayed a tiny fast secretory component, which can be appreciated from the example C_m trace in Figure 1*C*. When the C_m changes of $Ca_V1.3^{-/-}$ IHCs were scaled by a factor of 12.8 (re-

quired to match peak Ca^{2+} currents of wt and $Ca_V1.3^{-/-}$ IHCs) (Fig. 1*B*), the fast secretory components of IHCs from both genotypes overlapped (Fig. 1*D*, dashed line). This suggests that the residual Ca^{2+} channels of $Ca_V1.3^{-/-}$ IHCs couple to fast exocytosis with comparable efficacy, provided that the Ca^{2+} current linearly relates to RRP exocytosis (A. Brandt and T. Moser, unpublished observations).

If the reduced depolarization-stimulated exocytosis of $Ca_V1.3^{-/-}$ IHCs was solely attributable to the impaired Ca^{2+} influx, they should secrete normally when bypassing Ca^{2+} influx by direct elevation of Ca^{2+} at the release sites. Indeed, flash photolysis of caged Ca^{2+} stimulated robust ΔC_m in $Ca_V1.3^{-/-}$ IHCs (Fig. 1*E*), which displayed two kinetic components as previously described for wt mouse IHCs (Beutner et al., 2001). The total amplitude of the average ΔC_m response (1.88 ± 0.21 pF; $n = 9$ recordings) was not statistically distinguishable from the mean amplitude of the wt flash responses obtained in a previous study (1.52 ± 0.09 pF; $n = 68$ recordings; $p > 0.1$; amplitude was independent of the flash-induced $[Ca^{2+}]_i$ change of at least $>10\ \mu M$) (Beutner et al., 2001). Therefore, the secretory defect of $Ca_V1.3^{-/-}$ IHCs is not caused by a lack of fusion competent vesicles, but is probably caused by a reduced number of Ca^{2+} channel-coupled release sites. The Ca^{2+} sensitivity of exocytosis in $Ca_V1.3^{-/-}$ IHCs remains to be investigated in future experiments, including quantification of the flash-induced $[Ca^{2+}]_i$ change.

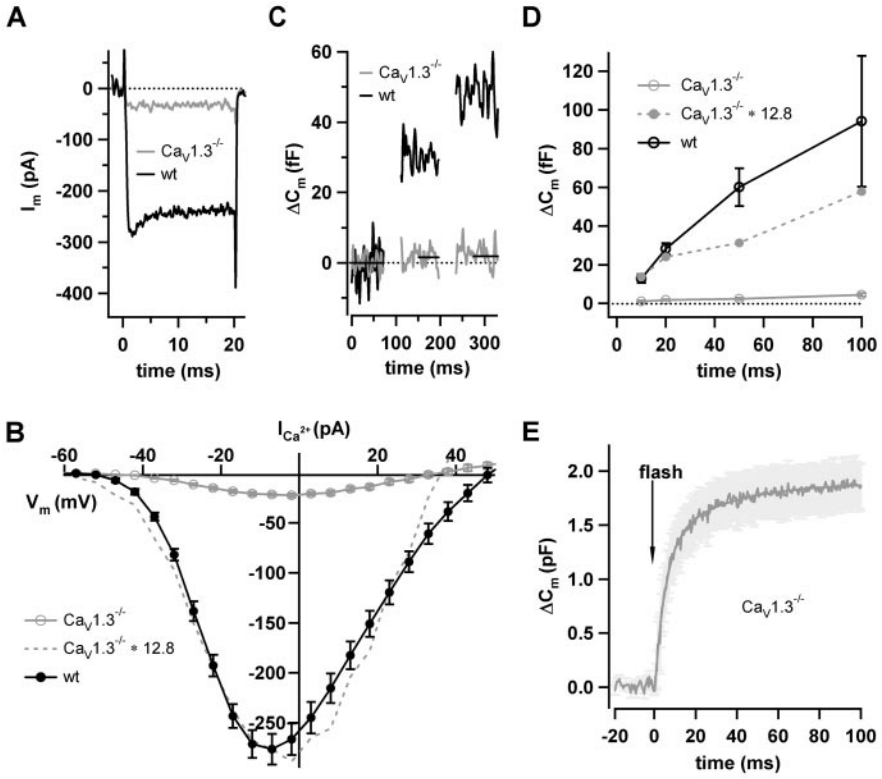

Figure 1. Strongly reduced Ca^{2+} current and exocytosis in $Ca_V1.3^{-/-}$ IHCs. *A* plots representative Ca^{2+} current traces for wt (P31) and $Ca_V1.3^{-/-}$ (P32) IHCs, which were elicited by step depolarization to the peak Ca^{2+} current potential (Solutions I_i and I_e were used for *A–D*). Data were leak-subtracted using a p/6 protocol. In *B* average current–voltage relationships (*I–V*) recorded from wt ($n = 6$ cells) and a $Ca_V1.3^{-/-}$ ($n = 7$ cells) IHCs are displayed. The dashed line represents a scaled version of the $Ca_V1.3^{-/-}$ *I–V* (scaling factor of 12.8 to match peak Ca^{2+} currents). *C, D,* Capacitance responses (ΔC_m) to paired depolarizations to the peak Ca^{2+} current potential, spaced 100 msec apart and having variable duration of 10, 20, 50, and 100 msec were recorded for wt ($n = 6$ cells; P20–P32) and $Ca_V1.3^{-/-}$ ($n = 9$ cells; P14–P32) IHCs. *C* shows representative examples of wt and $Ca_V1.3^{-/-}$ ΔC_m in response to a 2 * 20 msec paired pulse (low-pass filtered at 100 Hz). The bars indicate averages of baseline-subtracted $Ca_V1.3^{-/-}$ C_m over 400 msec before and 40–100 msec after the first and second depolarization. Intervals between the pairs were at least 30 sec to allow for complete recovery of the readily releasable pool (Moser and Beutner, 2000). *D* plots mean wt and mutant ΔC_m responses to the first depolarization versus the respective duration of the stimuli. *E* shows the average ΔC_m response of $Ca_V1.3^{-/-}$ IHCs ($n = 9$ recordings) to flash-photolysis of caged Ca^{2+}. The mean $Ca_V1.3^{-/-}$ ΔC_m is displayed along with its SE.

Developmental changes of Ca^{2+} current density: lack of postnatal electrical activity in $Ca_V1.3^{-/-}$ IHCs

Here, we tested the Ca^{2+} current density of wt and $Ca_V1.3^{-/-}$ IHCs at the end of the first week [postnatal day 6 (P6)], around and after the onset of hearing (P14–P32). $Ca_V1.3^{-/-}$ IHCs did not display the developmental increase of membrane capacitance, which is observed in wt IHCs (Table 1) (Beutner and Moser, 2001). This, probably, indicates that $Ca_V1.3^{-/-}$ IHCs do not increase in size during development. At any age, Ca^{2+} current density (Fig. 2*A*, top panel) and exocytosis (data not shown) of mutant cells were reduced to ~5–10% of control. The remaining Ca^{2+} current density of $Ca_V1.3^{-/-}$ IHCs showed a developmental decrease during the second postnatal week (Fig. 2*A*, bottom panel), as had been previously described for wt IHCs (NMRI mice) (Beutner and Moser, 2001).

AP firing takes place in immature IHCs of wt mice (Fig. 2*B*) but not in $Ca_V1.3^{-/-}$

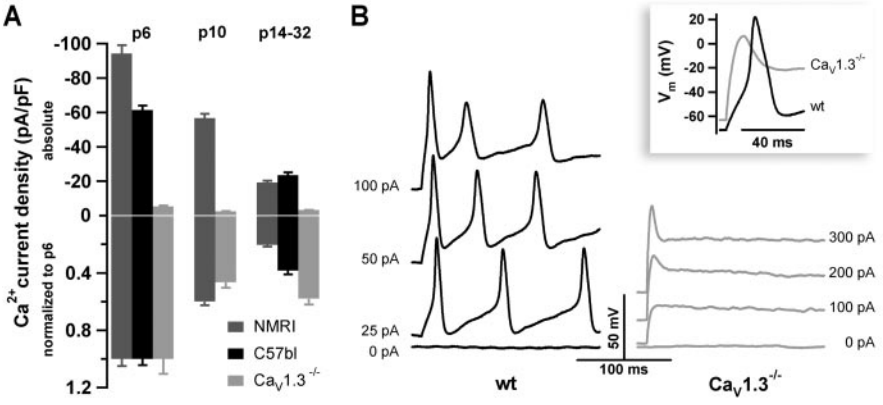

Figure 2. Developmental changes of Ca^{2+} current density: lack of Ca^{2+} spikes in $Ca_V1.3^{-/-}$ IHCs. *A* shows mean absolute (top panel) and normalized (bottom panel, normalized to P6 values) Ca^{2+} current densities for $Ca_V1.3^{-/-}$, C57BL/6J, and NMRI IHCs (the NMRI data set was taken from Beutner and Moser, 2001) at P6 ($n_{NMRI} = 10$; $n_{C57BL/6J} = 2$; $n_{Cav1.3^{-/-}} = 5$ IHCs), P10 ($n_{NMRI} = 9$; $n_{Cav1.3^{-/-}} = 7$ IHCs), and P14–P32 ($n_{NMRI} = 28$; $n_{C57BL/6J} = 8$; $n_{Cav1.3^{-/-}} = 8$ IHCs). The top panel highlights the dramatic reduction in Ca^{2+} current density in $Ca_V1.3^{-/-}$ IHCs. The bottom panel emphasizes the developmental current density reduction in all strains investigated. *B,* Whereas current injection readily triggered APs in wt IHCs (left panel, example is P5), even strong current injections failed to elicit APs in $Ca_V1.3^{-/-}$ IHCs (right panel, example is P7). The inset compares the initial rise of membrane potential of representative wt and $Ca_V1.3^{-/-}$ IHCs after injection of 300 pA.

IHCs. Current-clamp experiments were performed at the end of the first postnatal week, when the Ca^{2+} channel density is largest (Fig. 2*A*). In contrast to wt IHCs, we observed only passive membrane charging from a slightly more depolarized resting potential (Table 1) followed by a repolarization even during strong depolarizing current injections (Fig. 2*B*). The depolarized V_m was not caused by increased membrane leak in $Ca_V1.3^{-/-}$ IHCs (Table 1, R_{in}). Results similar to those of Figure 2*B* were obtained in 15 wt IHCs and 9 $Ca_V1.3^{-/-}$ IHCs. We conclude that the remaining Ca^{2+} current density was too low to support spiking in $Ca_V1.3^{-/-}$ IHCs.

Ca^{2+} channel types involved in the residual Ca^{2+} current of $Ca_V1.3^{-/-}$ IHCs

Next, we investigated which channel types mediate the residual Ca^{2+} current in $Ca_V1.3^{-/-}$ IHCs and how they contribute to stimulus–secretion coupling. To increase the current amplitude, Ba^{2+} (20 mM) was used as the permeating ion for the pharmacological dissection of the remaining Ca^{2+} channels. All experiments were performed between postnatal days 17 and 25. We first tested the presence of L-type Ca^{2+} channels using DHPs, because the voltage dependence and kinetics of the Ca^{2+} current were quite comparable between mutant and control IHCs (Fig. 1*A*,*B*). Figure 3*A* shows that the DHP agonist of L-type Ca^{2+} channels BayK8644 (5 μM; $n = 4$ IHCs), which prolongs the mean channel open time (Brown et al., 1984), strongly increased the Ca^{2+} current of mutant IHCs to ~270%. As expected, BayK8644 also shifted the activation to more hyperpolarized potentials. The Ba^{2+} current of mutant IHCs was inhibited by the potent DHP antagonist isradipine (10 μM; $n = 7$ IHCs) to ~40% of control (Fig. 3*A*). Application of the subtype-nonspecific blocker of voltage-gated Ca^{2+} channels Ni^{2+} (5 mM; $n = 2$ IHCs) (Fig. 3*A*) abolished DHP-insensitive Ba^{2+} current of $Ca_V1.3^{-/-}$ IHCs, showing that it was mediated by Ca^{2+} channels.

At our holding potential (−86 mV), $Ca_V1.2$ channels are more sensitive to isradipine (complete inhibition by submicromolar isradipine) than $Ca_V1.3$ channels (micromolar isradipine required for full inhibition) (Koschak et al., 2001). To test a potential contribution of $Ca_V1.2$ channels, we subsequently applied 200 nM and 5 μM isradipine while recording the Ca^{2+} currents and exocytic C_m changes (Fig. 3*B*) (depolarization to −6 mV, experiment is representative of two further perforated-patch experiments). The residual Ca^{2+} current and ΔC_m of $Ca_V1.3^{-/-}$ IHCs were only marginally affected by submicromolar isradipine (200 nM), arguing against a major contribution of $Ca_V1.2$ channels. In the presence of 5 μM isradipine ΔC_m were abolished, indicating that the remaining Ca^{2+} current did not induce exocytosis, exceeding our detection limit of ~1 fF (~30 fused vesicles, assuming a conversion factor of 37 aF per vesicle) (Lenzi et al., 1999).

We then used peptide toxins to probe the contributions of N- ($Ca_V2.2$), P/Q- ($Ca_V2.1$), and R-type ($Ca_V2.3$) Ca^{2+} channels to the Ba^{2+} current of $Ca_V1.3^{-/-}$ IHCs. Experiments were performed in both the perforated-patch and whole-cell configuration for each drug. Figure 3*C* shows averaged *I–V* relationships of a representative perforated-patch experiment in which subsequent application of ω-conotoxin GVIA (1 μM, inhibitor of $Ca_V2.2$) and ω-conotoxin MVIIC (3 μM, blocking both $Ca_V2.2$ and $Ca_V2.1$) failed to reduce the Ba^{2+} current of $Ca_V1.3^{-/-}$ IHCs. This observation was confirmed in three additional perforated-patch experiments (1 μM ω-conotoxin GVIA followed by 6 μM ω-conotoxin MVIIC).

Next, we investigated the presence of R-type ($Ca_V2.3$) Ca^{2+} channels by applying the specific toxin inhibitor SNX-482 (Tottene et al., 2000). No significant differences of peak Ba^{2+} currents were observed (1 μM SNX-482; $n = 6$ IHCs) (Fig. 3*D*). Interestingly, the inorganic Ca^{2+} channel blocker Ni^{2+} caused a significant inhibition of the Ca^{2+} current at a concentration of 50 μM (~60%; $n = 9$ IHCs) (Fig. 3*D*), at which Ni^{2+} has been shown to selectively inhibit R-type Ca^{2+} channels (Gasparini et al., 2001). Ni^{2+} and isradipine blocked similar amounts of the Ba^{2+} currents in $Ca_V1.3^{-/-}$ IHCs. Figure 3*D* summarizes the effects of DHPs, peptide toxins, and Ni^{2+} (50 μM and 5 mM) on the peak Ba^{2+} current of $Ca_V1.3^{-/-}$ IHCs. We compared test and control responses for each drug. The control data were mainly obtained from perforated-patch experiments before drug application. Together, these experiments show that the remaining Ca^{2+} current in $Ca_V1.3^{-/-}$ IHCs is mediated by L-type channels and, possibly, to a lesser extent by R-type channels.

Lack of functional large-conductance Ca^{2+}-activated K^+ channels

Mature wt IHCs displayed three distinct K^+ currents (Fig. 4), which is in agreement with previous reports (Marcotti et al., 2003; Oliver et al., 2003). Depolarization recruited fast and slow outward currents (Fig. 4*A*). The fast current showed submillisecond activation and was selectively inhibited by low doses of TEA (5 mM) (Fig. 4*B*), as has been previously described for $I_{K,f}$ in IHCs (Kros and Crawford, 1990). This current has been attributed to large-conductance Ca^{2+}-activated K^+ channels (BK channels; Langer et al., 2003). The slow outward current was less sensitive to TEA but primarily blocked by 4-aminopyridine (data not shown). This current has been termed $I_{K,s}$ (Kros and Crawford, 1990) and is thought to be carried by delayed rectifier (K_V) K^+ channels. When clamping mature IHCs close to their resting potential we observed a conductance, which inactivated during hyperpolarization (Fig. 4*E*) and was resistant to tetraethylammonium (TEA) and 4-aminopyridine (data not shown). This conductance was most likely mediated by KCNQ channels, which show low voltage activation and set the resting potential of IHCs (Marcotti et al., 2003; Oliver et al., 2003).

$Ca_V1.3^{-/-}$ IHCs lacked fast outward currents at any age that we investigated (up to P35). Figure 4*A* demonstrates the kinetic and amplitude differences between representative outward currents of wt (P25) and $Ca_V1.3^{-/-}$ (P30) IHCs. The lack of $I_{K,f}$ in $Ca_V1.3^{-/-}$ IHCs becomes even more obvious, when the currents are displayed normalized to their steady-state values (Fig. 4*B*). Currents of wt IHCs treated with 5 mM TEA and of $Ca_V1.3^{-/-}$ IHCs greatly overlapped, except for a small, unblocked $I_{K,f}$ component in the wt cells. We did not observe any effect of 5 mM TEA on the outward current of $Ca_V1.3^{-/-}$ IHCs (data not shown).

One might argue that the apparent lack of functional BK channels from $Ca_V1.3^{-/-}$ IHCs was attributable to the reduced voltage-gated Ca^{2+} influx, which, together with depolarization, normally coactivates the BK channels (Lewis and Hudspeth, 1983; Art and Fettiplace, 1987). However, we show here that elevation of $[Ca^{2+}]_i$ by loading Ca^{2+} through the patch pipette (1 mM), which was qualitatively confirmed by fura-2 $[Ca^{2+}]_i$ imaging (data not shown), did not reveal $I_{K,f}$ in $Ca_V1.3^{-/-}$ IHCs (Fig. 4*C*). In addition, we did not observe submillisecond current activation in $Ca_V1.3^{-/-}$ IHCs even at very depolarized potentials (+24 mV), at which $I_{K,f}$ in excised patches is also activated at low $[Ca^{2+}]$ (Oliver et al., 2003). We conclude that $Ca_V1.3^{-/-}$ IHCs lack functional BK channels. *I–V* relationships from wt ($n = 5$ IHCs; P24–P29), wt + 5 mM TEA ($n = 2$ IHCs; P24, P29) and $Ca_V1.3^{-/-}$ (high Ca^{2+}; $n = 5$ IHCs; P25) IHCs were obtained by

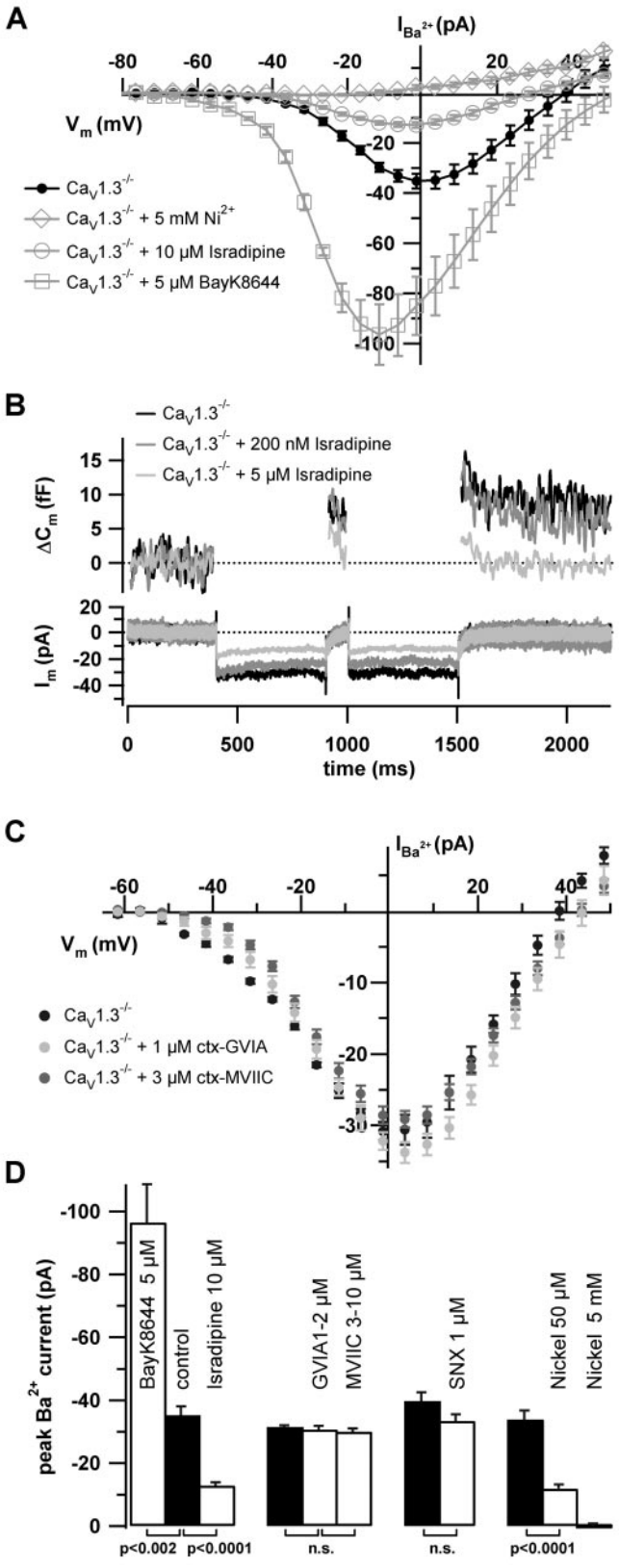

Figure 3. Identity and function of the Ca^{2+} channels in $Ca_V1.3^{-/-}$ IHCs. *A* plots average Ba^{2+} current IVs (mean ± SEM) of mutant IHCs under control conditions and during application of the DHP agonist BayK8644 (5 µM; $n = 4$ cells), the DHP antagonist isradipine (10 µM; $n = 7$ cells), or nickel (5 mM; $n = 2$ cells). Control *I–V* relationships before application of DHP agonists and antagonists were pooled. Individual *I–V* relationships were leak-corrected (see Materials and Methods). *B* compares leak-corrected Ca^{2+} currents and corresponding ΔC_m recorded in the perforated-patch configuration in response to pairs of 500 msec depolarizations to −6 mV during subsequent treatment with 200 nM and 5 µM of isradipine. *C* plots average Ba^{2+} current *I–V* relationships of a representative perforated-patch experiment in which application of 1 µM of ω-conotoxin (ctx) GVIA was followed by wash-in of 3 µM of ω-conotoxin MVIIC without any obvious effects on current amplitude or voltage dependence. *D* summarizes the mean effects of the specified drugs on the $Ca_V1.3^{-/-}$ IHCs peak Ba^{2+} current. Each group of drugs was compared with their own control data acquired in perforated-patch experiments before the wash-in of the drug. The error probabilities for assuming statistically different mean amplitudes are provided underneath the plot.

time window analysis (Fig. 4*D*) and by exponential fitting (data not shown) to quantitatively confirm this finding. Traces of wt cells recorded at potentials positive to −45 mV were best fit by the sum of two exponential functions [activation time constants of the fast current component ($I_{K,f}$) were <1 msec; those of the slow current components ($I_{K,s}$) > 5 msec]. Traces of mutant hair cells were reasonably well described by single exponential functions, with time constants of activation similar to $I_{K,s}$ of wt cells. Current amplitudes of $Ca_V1.3^{-/-}$ IHCs and TEA-treated wt cells were similar (Fig. 4*B,D*), despite the much smaller C_m of $Ca_V1.3^{-/-}$ IHCs (Table 1), arguing for a compensatory increase of K_V current density.

$Ca_V1.3^{-/-}$ IHCs also showed KCNQ currents (Fig. 4*E*). Analysis of the deactivating current component measured after stepping from −65 to −125 mV (after 1.5 msec and at steady-state) revealed comparable mean current densities and deactivation time constants of wt (7.99 ± 0.79 pA/pF; 17.4 ± 1.3 msec; $n = 6$ cells; P25) and $Ca_V1.3^{-/-}$ (9.55 ± 2.8 pA/pF; 22.1 ± 2.6 msec; $n = 9$ cells; P24–P25) IHCs. Together, these experiments indicate that $Ca_V1.3$ deficiency causes a selective lack of functional BK channels and a compensatory increase of the membrane density of K_V channels.

Persistence of cholinergic postsynaptic currents in $Ca_V1.3^{-/-}$ IHCs

Here, we studied the developmental changes of efferent synaptic signaling in both $Ca_V1.3^{-/-}$ and wt IHCs under resting conditions and during high $[K^+]_e$ stimulation. As shown in Figure 5*A*, spontaneous postsynaptic currents were readily observed in both groups at the end of the first postnatal week. At holding potentials negative to $E_K{}^+$ (−80 mV), the postsynaptic signals were inward currents. At intermediate potentials (slightly positive to $E_K{}^+$), these signals were composed of a brief, initial inward current followed by a long-lasting outward current (Fig. 5*A,C*). Figure 5*B* displays average current–voltage relationships of the slow current component recorded from P6 wt IHCs ($n = 3$ cells) as well as from P6 ($n = 2$ cells) and P35 ($n = 3$ cells) $Ca_V1.3^{-/-}$ IHCs, with all currents reversing near $E_K{}^+$. We did not obtain any postsynaptic currents in recordings from control IHCs at P25 despite high K^+ stimulation (10 mM KCl; $n = 3$ cells; data not shown), which is in line with a previous study on rat IHCs (Glowatzki and Fuchs, 2000). On the contrary, every $Ca_V1.3^{-/-}$ IHC tested ($n = 14$ cells; up to P35) displayed spontaneous postsynaptic currents (Fig. 5*A*). Figure 5, *E* and *F*, shows for a representative experiment that these persistent, postsynaptic currents were inhibited by 300 nM strychnine, blocker of the α9-receptor (Elgoyhen et al., 1994) or 1 µM dequalinium, blocker of small-conductance Ca^{2+}-activated K^+ channels (SK) (Strobaek et al., 2000). These findings were confirmed in three more P30–P35 $Ca_V1.3^{-/-}$ IHCs. In addition, the single event characteristics were comparable among P6 wt IHCs and $Ca_V1.3^{-/-}$ IHCs at P6 and P35 (Table 2). Thus, our data suggest that the postsynaptic currents of p35 $Ca_V1.3^{-/-}$ IHCs are mediated by the same mechanism as in chick cochlear

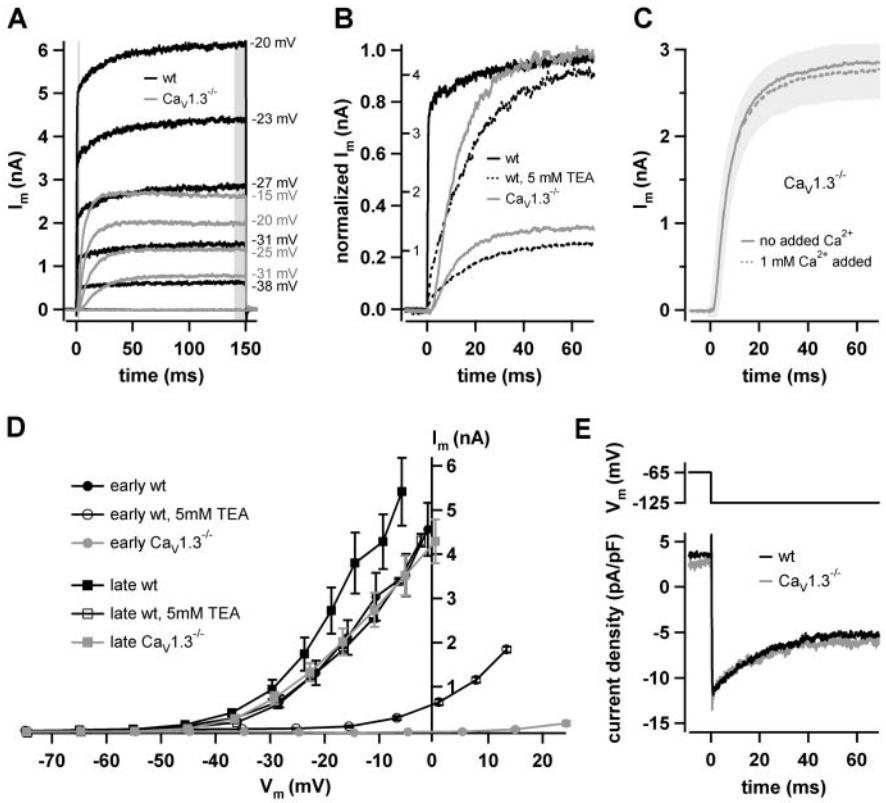

Figure 4. Lack of functional large-conductance Ca^{2+}-activated K^+ channels in $Ca_V1.3^{-/-}$ IHC. *A* compares representative current traces of wt (P25) and mutant (P30) IHCs evoked by 150-msec-long step depolarizations to the indicated potentials. In *B* example traces of wt (−23 mV), wt + 5 mM TEA (−23 mV), and $Ca_V1.3^{-/-}$ (−25 mV) IHCs are shown on expanded time scale after normalizing them to their steady-state values reached at the end of the depolarization (outside axis, steady-state values were not reached within the displayed time frame, but see Fig. 4*A*) as well as in absolute numbers (inside axis). Normalized and absolute currents of wt overlap. *C* shows averaged current traces (mean ± SEM) obtained from $Ca_V1.3^{-/-}$ IHCs after depolarization to −8 mV, which had either low (no added Ca^{2+}; 0.1 mM free EGTA in the pipette; $n = 3$ IHCs) or high (1 mM added Ca^{2+}; no EGTA in the pipette; $n = 5$ IHCs) basal $[Ca^{2+}]_i$. For the latter, the change of intracellular $[Ca^{2+}]_i$ was qualitatively confirmed by fura-2 fluorimetry (data not shown). *D* displays average *I–V* relationships for wt ($n = 5$ IHCs; P24–P29), wt + 5 mM TEA ($n = 2$ IHCs; P24, P29), and $Ca_V1.3^{-/-}$ (high Ca^{2+}; $n = 5$ IHCs; P25) IHCs. "Early" and "late" designate the averaging time windows (shown as gray bars in *A*) of 1.2 msec for 100 μsec (mainly representing $I_{K,f}$ in wt) and 140 msec for 9.5 msec (representing the sum of all outward currents), respectively. *E* plots representative current density traces obtained from wt and mutant IHCs during a hyperpolarizing voltage step from −65 to −125 mV. The mean series resistance of all cells included in Figure 4 was 5.6 ± 0.3 MΩ after R_s compensation and data were off-line-corrected for the remaining voltage error.

hair cells, mammalian outer hair cells, and immature wt IHCs (Fuchs and Murrow, 1992; Glowatzki and Fuchs, 2000; Oliver et al., 2000): transient cholinergic Ca^{2+} influx into the IHCs causing K^+ current through SK channels. Figure 5*D* shows that these postsynaptic currents induced a brief depolarization followed by a long hyperpolarization in resting P35 $Ca_V1.3^{-/-}$ IHCs.

Mechanoelectrical transduction is functional in $Ca_V1.3^{-/-}$ IHCs

Next, we investigated whether mechanoelectrical transduction (MET) was also impaired in the absence of $Ca_V1.3$. Stereociliar deflection was achieved by a fluid-jet that was driven by a sinusoidal voltage signal. Transduction currents were clearly present in $Ca_V1.3^{-/-}$ IHCs. For each recorded cell, driving voltage and proximity of the fluid jet were optimized to gain the cells' maximum MET response. Mean peak transduction currents (P6, holding potential: −75 mV; 60 Hz stimulation) were −104 ± 16.4 pA for $Ca_V1.3^{-/-}$ ($n = 5$ cells) and −99.9 ± 10.0 pA for wt ($n = 7$ cells) IHCs. Smaller amplitudes were observed in p30 wt and $Ca_V1.3^{-/-}$ IHCs.

Discussion

IHCs from $Ca_V1.3$ knock-out mice showed a near complete block of depolarization-induced exocytosis. Our analysis demonstrated that major features of hair cell development, such as the acquisition of large-conductance Ca^{2+}-activated K^+ channels, require an abundance of $Ca_V1.3$ channels. On the other hand, mechanoelectrical transduction currents and K^+ currents mediated by K_V and KCNQ channels were present in $Ca_V1.3^{-/-}$ IHCs. This argues against a global degeneration of IHCs caused by the channelopathy within the time frame investigated. In conclusion, $Ca_V1.3$ channels are not only essential for afferent synaptic transmission but also contribute to the regulation of hair cell development.

Role of $Ca_V1.3$ channels in stimulus–secretion coupling of IHCs

The Ca^{2+} current of $Ca_V1.3^{-/-}$ IHCs amounted to only ~8% of the total Ca^{2+} current measured in IHCs of hearing wt mice (Fig. 1*A*,*B*). This is similar to the current reduction observed in IHCs from early postnatal $Ca_V1.3^{-/-}$ mice (Platzer et al., 2000). Depolarization-induced exocytosis of $Ca_V1.3^{-/-}$ IHCs was strongly decreased (Fig. 1*C*,*D*), confirming the essential role of Ca^{2+} influx for hair cell transmitter release (Moser and Beutner, 2000; Spassova et al., 2001). Exocytosis was abolished when $Ca_V1.3^{-/-}$ IHCs were treated with micromolar concentrations of the DHP antagonist isradipine (Fig. 3*B*), which also blocks most of the Ca^{2+} current in wt IHCs (Brandt and Moser, unpublished data). The presence of a small number of rapidly released vesicles indicates that L-type Ca^{2+} channels remaining after $Ca_V1.3$ ablation couple as efficiently to exocytosis as $Ca_V1.3$ itself. We suggest that the strong inhibition of IHC transmitter release, which itself is a sufficient reason for the deafness of the mutant, is caused by a reduction of presynaptic Ca^{2+} channel-coupled release sites.

Flash photolysis of caged Ca^{2+} elicited normal exocytic responses (Fig. 1*E*). This finding of a normal number of fusion competent vesicles is striking, given that recent morphological data suggest a major reduction of synaptic ribbons in $Ca_V1.3^{-/-}$ IHCs (Glueckert et al., 2003). It has been suggested that synaptic ribbons are involved in sustained transmitter release from sensory synapses as well as in the exocytic responses to flash photolysis (Lenzi and von Gersdorff, 2001). Possible explanations of our finding include: (1) a selective defect of exocytosis caused by the reduction of Ca^{2+} channel-coupled release sites (see above) with a normal population of fusion competent vesicles (docked at and/or outside the active zone), (2) the presence of a large-scale exocytic process that is not

related to synaptic transmission. Future measurements of glutamate release from $Ca_V1.3^{-/-}$ IHCs (Glowatzki and Fuchs, 2002) will be needed to distinguish between these possibilities.

The Ca^{2+} channel-set of the cochlear inner hair cell

The incomplete blockade of hair cell Ca^{2+} currents by various DHP antagonists of L-type Ca^{2+} channels has left some uncertainty about the presence of non-L-type Ca^{2+} channels and their potential contribution to transmitter release (Fuchs et al., 1990; Moser and Beutner, 2000; Rodriguez-Contreras and Yamoah, 2001; Spassova et al., 2001). The initial analysis of $Ca_V1.3^{-/-}$ mice (Platzer et al., 2000) had demonstrated that $Ca_V1.3$ is the predominant Ca^{2+} channel of immature mouse cochlear IHCs. Here, we took advantage of $Ca_V1.3^{-/-}$ mice to demonstrate that $Ca_V1.3$ also dominates the Ca^{2+} current of IHCs in older mice (~92%). The apparent discrepancy of the pharmacological and genetic approaches can be reconciled if the voltage dependence of DHP action on $Ca_V1.3$ is considered (Koschak et al., 2001).

We then used the $Ca_V1.3^{-/-}$ mice to study the contribution of other Ca^{2+} channels in more detail (Fig. 3). From our pharmacological analysis we conclude that ~60% of the residual Ca^{2+} current is mediated by L-type channels. Involvement of $Ca_V1.1$ channels is unlikely, because $Ca_V1.1$ activates extremely slowly. Also $Ca_V1.2$ seems not to contribute substantially, because we observed only marginal effects of 200 nM isradipine, whereas 300 nM completely blocks $Ca_V1.2$ channels (Koschak et al., 2001). $Ca_V1.4$ remains an attractive candidate for several reasons: (1) it is robustly stimulated by BayK 8644 and requires micromolar concentrations of isradipine for full blockade (Koschak et al., 2003); (2) $Ca_V1.4$ $\alpha1$ subunits are expressed in sensory cells (retinal photoreceptor), where they must also be able to tightly couple to neurotransmitter release (Bech-Hansen et al., 1998; Strom et al., 1998); (3) $Ca_V1.4$ channels inactivate very slowly, similar to the L-type current component in $Ca_V1.3^{-/-}$ mice reported here. This needs to be confirmed in future biochemical studies of Ca^{2+} channel subunit expression.

None of the subtype-specific peptide toxins, ω-conotoxin GVIA, ω-conotoxin MVIIC, and SNX-482 significantly blocked the DHP-insensitive Ca^{2+} current of $Ca_V1.3^{-/-}$ IHCs. The inhibition by low micromolar Ni^{2+} could indicate that it was mediated by R-type channels (Gasparini et al., 2001), which then had to be insensitive to SNX-482. Highly Ni^{2+}-sensitive R-type current components with varying SNX-482 sensitivity have previously been described (Sochivko et al., 2002). In conclusion, IHCs in addition to $Ca_V1.3$ contain a small number of further L-type channels of currently unknown molecular identity. A very small fraction of the Ca^{2+} current of the IHCs might be mediated by SNX-482-insensitive R-type channels. N- and P/Q-type Ca^{2+} channels do not contribute.

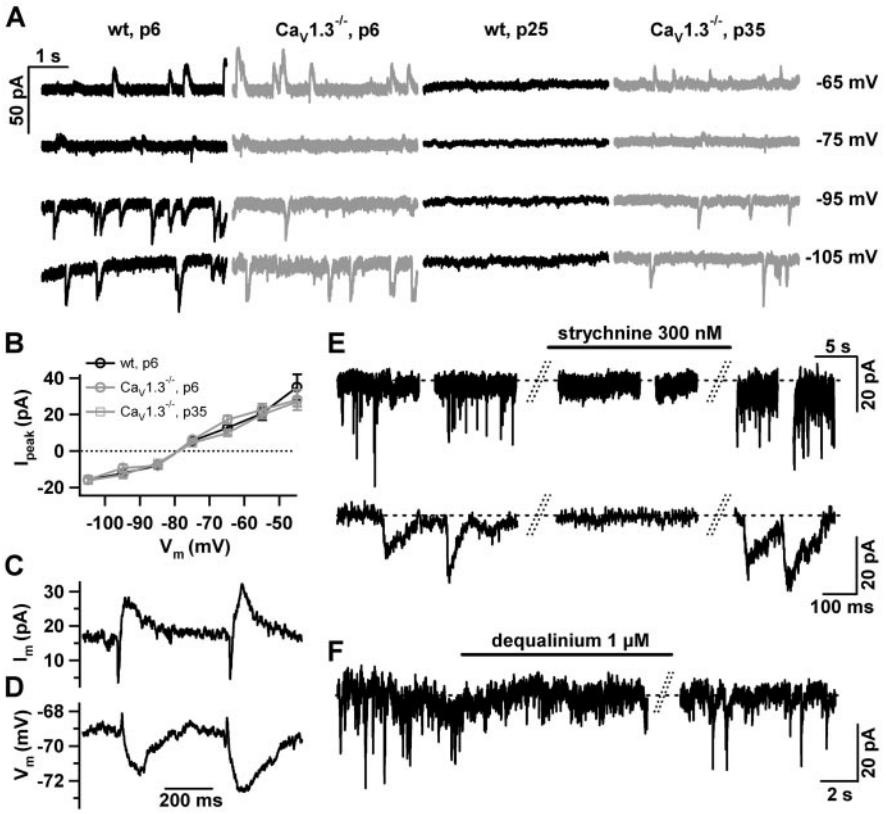

Figure 5. Continued presence of postsynaptic responses in $Ca_V1.3^{-/-}$ IHCs. *A* compares representative spontaneous postsynaptic currents of wt and $Ca_V1.3^{-/-}$ IHCs before and after the onset of hearing in wt (potentials are indicated next to the traces). *I–V* relationships of the slow component of the postsynaptic currents are plotted in *B*. *C* displays biphasic postsynaptic currents of a P30 $Ca_V1.3^{-/-}$ IHC (at −75 mV) in more detail. *D* shows a stretch of a current-clamp V_m recording from the same cell as in *C*, illustrating the depolarizing onset and hyperpolarizing main component of these postsynaptic potentials. Extracellular application of 300 nM strychnine (P35; *E*) and dequalinium (1 μM; *F*; same cell as in *E*) abolished the postsynaptic currents of $Ca_V1.3^{-/-}$ IHCs. The inhibitory effects of both drugs were reversible.

Impairment of hair cell development in the absence of $Ca_V1.3^{-/-}$

$Ca_V1.3^{-/-}$ IHCs do not generate Ca^{2+} action potentials (Fig. 2*B*), which are a hallmark of normal IHC development (Kros et al., 1998; Glowatzki and Fuchs, 2000; Beutner and Moser, 2001). The lack of Ca^{2+} action potentials might be at the origin of some of the observed developmental defects. Ca^{2+} action potentials drive presensory hair cell exocytosis (Beutner and Moser, 2001) of glutamate (Glowatzki and Fuchs, 2002) and possibly neurotrophic factors (for review, see Rubel and Fritzsch, 2002), which is probably required for synaptogenesis and maintenance of afferent synapses and neurons during development. Indeed, the first signs of afferent dendrite degeneration are visible by electron microscopy of $Ca_V1.3^{-/-}$ organs of Corti already at the end of the first postnatal week (Glueckert et al., 2003). It is likely that the defective afferent synaptic transmission and the subsequent degeneration of afferent dendrites lead to the persistent olivocochlear cholinergic input into $Ca_V1.3^{-/-}$IHCs (Glueckert et al., 2003) (Fig. 5). The signaling mechanism that causes efferent terminals to give up their axosomatic synaptic contacts with IHCs and to form axodendritic synapses with the afferent fibers during normal development remains to be characterized.

Postnatal Ca^{2+} spikes or the presence of $Ca_V1.3$ channels in

Table 2. Analysis of postsynaptic currents

	Peak amplitude at −90 mV (pA)	Peak amplitude at −40 mV (pA)	Halfwidth at −90 mV (msec)	Charge at −90 mV (pC)
wt, P6	−11.3 ± 2.42 ($n = 40$)	31.1 ± 8.53 ($n = 15$)	54.0 ± 1.74 ($n = 36$)	0.71 ± 0.21 ($n = 15$)
$Ca^v1.3^{-/-}$, P6	−11.5 ± 0.32 ($n = 445$)	23.3 ± 1.83 ($n = 95$)	43.2 ± 1.04 ($n = 410$)	0.54 ± 0.02 ($n = 77$)
$Ca_v1.3^{-/-}$, P35	−10.0 ± 0.51 ($n = 79$)	15.8 ± 2.20 ($n = 42$)	31.4 ± 1.74 ($n = 79$)	0.34 ± 0.04 ($n = 36$)

Peaks had to exceed at least three times the SD of the actual current trace to be accepted and were analyzed by a custom software programmed in IgorPro.

the plasma membrane itself are essential for the acquisition of functional BK channels during hair cell development. It is unlikely that experimental conditions prevented the detection of BK currents in $Ca_V1.3^{-/-}$ IHCs. We never observed submillisecond activation of outward currents in $Ca_V1.3^{-/-}$ IHCs even at very depolarized potentials (+24 mV) and did not find any change in activation kinetics after including 1 mM Ca^{2+} into the pipette. Therefore, the absence of BK current in $Ca_V1.3^{-/-}$ IHCs reflects a lack of functional BK channels rather than a defective BK channel activation caused by reduced Ca^{2+} influx.

The regenerative $[Ca^{2+}]$ changes of immature IHCs could coregulate the BK channel expression together with thyroid hormone (which is normal in $Ca_V1.3^{-/-}$ mice; Platzer et al., 2000). However, it currently seems more likely that the lack of BK current in $Ca_V1.3^{-/-}$ IHCs is not caused by defective gene expression. Preliminary data obtained by *in situ* hybridization suggests the presence of BK channel mRNA in $Ca_V1.3^{-/-}$ IHCs (Waka et al., 2003). Alternatively, BK channels may not get sufficiently targeted or anchored at the hair cell plasma membrane in the absence of $Ca_V1.3$. Future experiments will be required to clarify the exact mechanism by which $Ca_V1.3$ Ca^{2+} channels regulate the abundance of functional BK channels in IHCs.

Clinical implications of the $Ca_V1.3^{-/-}$ phenotype

So far, no human hereditary deafness has been reported to result from a channelopathy of $Ca_V1.3$. This is in contrast to the visual system, where mutations in the gene coding for the retinal L-type Ca^{2+} channel ($Ca_V1.4$) cause X-linked congenital stationary night blindness (Bech-Hansen et al., 1998; Strom et al., 1998). Defects of IHCs, their synapses or the auditory nerve are believed to cause a specific type of hearing impairment called auditory neuropathy. It includes a large variety of pathological conditions ranging from hereditary IHC lesions to demyelinating disease (Doyle et al., 1998; Brown and Dort, 2001; Lesinski-Schiedat et al., 2001; Varga et al., 2003). The "early" $Ca_V1.3^{-/-}$ mouse resembles a synaptic model of auditory neuropathy, as the blockade of hair cell afferent synaptic transmission represents the primary defect before degeneration of afferent fibers and outer hair cells eventually occurs. Further genetic analysis of hearing-impaired families will be required to explore whether mutations in the gene coding for $Ca_V1.3$ cause human auditory neuropathy.

References

Art JJ, Fettiplace R (1987) Variation of membrane properties in hair cells isolated from the turtle cochlea. J Physiol (Lond) 385:207–242.

Bech-Hansen NT, Naylor MJ, Maybaum TA, Pearce WG, Koop B, Fishman GA, Mets M, Musarella MA, Boycott KM (1998) Loss-of-function mutations in a calcium-channel alpha1-subunit gene in Xp11.23 cause incomplete X-linked congenital stationary night blindness. Nat Genet 19:264–267.

Beutner D, Moser T (2001) The presynaptic function of mouse cochlear inner hair cells during development of hearing. J Neurosci 21:4593–4599.

Beutner D, Voets T, Neher E, Moser T (2001) Calcium dependence of exocytosis and endocytosis at the cochlear inner hair cell afferent synapse. Neuron 29:681–690.

Brown AM, Kunze DL, Yatani A (1984) The agonist effect of dihydropyridines on Ca channels. Nature 311:570–572.

Brown DK, Dort JC (2001) Auditory neuropathy: when test results conflict. J Otolaryngol 30:46–51.

Bruce LL, Christensen MA, Warr WB (2000) : Postnatal development of efferent synapses in the rat cochlea. J Comp Neurol 423:532–548.

Dolmetsch RE, Xu K, Lewis RS (1998) Calcium oscillations increase the efficiency and specificity of gene expression. Nature 392:933–936.

Doyle KJ, Sininger Y, Starr A (1998) Auditory neuropathy in childhood. Laryngoscope 108:1374–1377.

Elgoyhen AB, Johnson DS, Boulter J, Vetter DE, Heinemann S (1994) Alpha 9: an acetylcholine receptor with novel pharmacological properties expressed in rat cochlear hair cells. Cell 79:705–715.

Elgoyhen AB, Vetter DE, Katz E, Rothlin CV, Heinemann SF, Boulter J (2001) alpha10: a determinant of nicotinic cholinergic receptor function in mammalian vestibular and cochlear mechanosensory hair cells. Proc Natl Acad Sci USA 98:3501–3506.

Eybalin M, Renard N, Aure F, Safieddine S (2002) Cysteine-string protein in inner hair cells of the organ of Corti: synaptic expression and upregulation at the onset of hearing. Eur J Neurosci 15:1409–1420.

Fuchs PA, Murrow BW (1992) A novel cholinergic receptor mediates inhibition of chick cochlear hair cells. Proc R Soc Lond B Biol Sci 248:35–40.

Fuchs PA, Evans MG, Murrow BW (1990) Calcium currents in hair cells isolated from the cochlea of the chick. J Physiol (Lond) 429:553–568.

Gasparini S, Kasyanov AM, Pietrobon D, Voronin LL, Cherubini E (2001) Presynaptic R-type calcium channels contribute to fast excitatory synaptic transmission in the rat hippocampus. J Neurosci 21:8715–8721.

Glowatzki E, Fuchs PA (2000) Cholinergic synaptic inhibition of inner hair cells in the neonatal mammalian cochlea. Science 288:2366–2368.

Glowatzki E, Fuchs PA (2002) Transmitter release at the hair cell ribbon synapse. Nat Neurosci 5:147–154.

Glueckert R, Wietzorrek G, Kammen-Jolly K, Scholtz A, Stephan K, Striessnig J, Schrott-Fischer A (2003) Role of class D L-type $Ca^{(2+)}$ channels for cochlear morphology. Hear Res 178:95–105.

Housley GD, Ashmore JF (1991) Direct measurement of the action of acetylcholine on isolated outer hair cells of the guinea pig cochlea. Proc R Soc Lond B Biol Sci 244:161–167.

Koschak A, Reimer D, Huber I, Grabner M, Glossmann H, Engel J, Striessnig J (2001) alpha 1D (Cav1.3) subunits can form l-type Ca^{2+} channels activating at negative voltages. J Biol Chem 276:22100–22106.

Koschak A, Reimer D, Walter D, Hoda JC, Heinzle T, Grabner M, Striessnig J (2003) Cav1.4alpha1 subunits can form slowly inactivating dihydropyridine-sensitive L-type Ca^{2+} channels lacking Ca^{2+}-dependent inactivation. J Neurosci 23:6041–6049.

Kros CJ, Crawford AC (1990) Potassium currents in inner hair cells isolated from the guinea-pig cochlea. J Physiol (Lond) 421:263–291.

Kros CJ, Ruppersberg JP, Rusch A (1998) Expression of a potassium current in inner hair cells during development of hearing in mice. Nature 394:281–284.

Langer P, Grunder S, Rusch A (2003) Expression of Ca^{2+}-activated BK channel mRNA and its splice variants in the rat cochlea. J Comp Neurol 455:198–209.

Lenzi D, von Gersdorff H (2001) Structure suggests function: the case for synaptic ribbons as exocytotic nanomachines. Bioessays 23:831–840.

Lenzi D, Runyeon JW, Crum J, Ellisman MH, Roberts WM (1999) Synaptic vesicle populations in saccular hair cells reconstructed by electron tomography. J Neurosci 19:119–132.

Lesinski-Schiedat A, Frohne C, Hemmaouil I, Battmer RD, Lenarz T (2001) Subjective deafness in case of peri-synaptic audiopathy. Isolated defects of the inner haircells? Laryngorhinootologie 80:601–604.

Lewis RS, Hudspeth AJ (1983) Voltage- and ion-dependent conductances in solitary vertebrate hair cells. Nature 304:538–541.

Lindau M, Neher E (1988) Patch-clamp techniques for time-resolved capacitance measurements in single cells. Pflügers Arch 411:137–146.

Lippe WR (1994) Rhythmic spontaneous activity in the developing avian auditory system. J Neurosci 14:1486–1495.

Marcotti W, Johnson SL, Holley MC, Kros CJ (2003) Developmental changes in the expression of potassium currents of embryonic, neonatal and mature mouse inner hair cells. J Physiol (Lond) 548:383–400.

Meyer J, Furness DN, Zenner HP, Hackney CM, Gummer AW (1998) Evidence for opening of hair-cell transducer channels after tip-link loss. J Neurosci 18:6748–6756.

Moser T, Beutner D (2000) Kinetics of exocytosis and endocytosis at the cochlear inner hair cell afferent synapse of the mouse. Proc Natl Acad Sci USA 97:883–888.

Mostafapour SP, Cochran SL, Del Puerto NM, Rubel EW (2000) Patterns of cell death in mouse anteroventral cochlear nucleus neurons after unilateral cochlea removal. J Comp Neurol 426:561–571.

Oliver D, Klocker N, Schuck J, Baukrowitz T, Ruppersberg JP, Fakler B (2000) Gating of Ca^{2+}-activated K+ channels controls fast inhibitory synaptic transmission at auditory outer hair cells. Neuron 26:595–601.

Oliver D, Knipper M, Derst C, Fakler B (2003) Resting potential and submembrane calcium concentration of inner hair cells in the isolated mouse cochlea are set by KCNQ-type potassium channels. J Neurosci 23:2141–2149.

Platzer J, Engel J, Schrott-Fischer A, Stephan K, Bova S, Chen H, Zheng H, Striessnig J (2000) Congenital deafness and sinoatrial node dysfunction in mice lacking class D L-type Ca^{2+} channels. Cell 102:89–97.

Pujol R (1985) Morphology, synaptology and electrophysiology of the developing cochlea. Acta Otolaryngol Suppl 421:5–9.

Roberts WM, Jacobs RA, Hudspeth AJ (1990) Colocalization of ion channels involved in frequency selectivity and synaptic transmission at presynaptic active zones of hair cells. J Neurosci 10:3664–3684.

Rodriguez-Contreras A, Yamoah EN (2001) Direct measurement of single-channel $Ca^{(2+)}$ currents in bullfrog hair cells reveals two distinct channel subtypes. J Physiol (Lond) 534:669–689.

Rubel EW, Fritzsch B (2002) Auditory system development: primary auditory neurons and their targets. Annu Rev Neurosci 25:51–101.

Rusch A, Erway LC, Oliver D, Vennstrom B, Forrest D (1998) Thyroid hormone receptor beta-dependent expression of a potassium conductance in inner hair cells at the onset of hearing. Proc Natl Acad Sci USA 95:15758–15762.

Simmons DD, Moulding HD, Zee D (1996) Olivocochlear innervation of inner and outer hair cells during postnatal maturation: an immunocytochemical study. Brain Res Dev Brain Res 95:213–226.

Sochivko DPA, Smyth N, Gissel C, Schneider T, Beck H (2002) The Ca(V)2.3 $Ca^{(2+)}$ channel subunit contributes to R-type Ca(2+) currents in murine hippocampal and neocortical neurones. J Physiol (Lond) 542:699–710.

Spassova M, Eisen MD, Saunders JC, Parsons TD (2001) Chick cochlear hair cell exocytosis mediated by dihydropyridine-sensitive calcium channels. J Physiol (Lond) 535:689–696.

Spitzer NC, Olson E, Gu X (1995) Spontaneous calcium transients regulate neuronal plasticity in developing neurons. J Neurobiol 26:316–324.

Strobaek D, Jorgensen TD, Christophersen P, Ahring PK, Olesen SP (2000) Pharmacological characterization of small-conductance $Ca^{(2+)}$-activated $K^{(+)}$ channels stably expressed in HEK 293 cells. Br J Pharmacol 129:991–999.

Strom TM, Nyakatura G, Apfelstedt-Sylla E, Hellebrand H, Lorenz B, Weber BH, Wutz K, Gutwillinger N, Ruther K, Drescher B, Sauer C, Zrenner E, Meitinger T, Rosenthal A, Meindl A (1998) An L-type calcium-channel gene mutated in incomplete X-linked congenital stationary night blindness. Nat Genet 19:260–263.

Tierney TS, Russell FA, Moore DR (1997) Susceptibility of developing cochlear nucleus neurons to deafferentation-induced death abruptly ends just before the onset of hearing. J Comp Neurol 378:295–306.

Tottene A, Volsen S, Pietrobon D (2000) alpha(1E) subunits form the pore of three cerebellar R-type calcium channels with different pharmacological and permeation properties. J Neurosci 20:171–178.

Varga R, Kelley PM, Keats BJ, Starr A, Leal SM, Cohn E, Kimberling WJ (2003) Non-syndromic recessive auditory neuropathy is the result of mutations in the otoferlin (OTOF) gene. J Med Genet 40:45–50.

Waka N, Langer P, Rusch A, Mcenery MW, Platzer J, Striessnig J, Engel J (2003) Extrasynaptic colocalization of and interaction between Cav1.3 and BK channels in mouse inner hair cells. ARO midwinter meeting. Daytona Beach, FL, February.

Walsh EJ, McGee J, McFadden SL, Liberman MC (1998) Long-term effects of sectioning the olivocochlear bundle in neonatal cats. J Neurosci 18: 3859–3869.